

Resonance formation of hydrogenic levels in front of metal surfaces

P. Kürpick and U. Thumm

J. R. Macdonald Laboratory, Department of Physics, Kansas State University, Manhattan, Kansas 66506-2604

U. Wille

Bereich Theoretische Physik, Hahn-Meitner-Institut Berlin, D-14091 Berlin, Germany

(Received 28 October 1996; revised manuscript received 26 February 1997)

The electronic self-energy of hydrogenic ions interacting with a jellium metal surface is studied within the fixed-ion approximation. A model framework is introduced that allows for the efficient computation of the complex (non-Hermitian) self-energy matrix in a large space of (bound) hydrogenic states. For the specific case of protons interacting with an aluminum surface, resonance energies and widths of dressed ionic states are obtained by diagonalizing the self-energy matrix. The hybridization properties of the dressed ionic states are analyzed. The self-energy of individual dressed states is found to converge rapidly with increasing dimension of the space of unperturbed hydrogen states. The resonance energies are compared to (1) energies obtained by diagonalizing only the direct couplings among the hydrogen states and (2) the real part of the diabatic (diagonal) self-energy. This comparison demonstrates the pronounced effect that indirect couplings between hydrogen states via conduction band states have on the resonance energies at intermediate and small ion-surface distances. Our results for incident protons are confronted with the results of other (perturbative and nonperturbative) calculations of level shifts and widths in proton-surface interactions. Although we use a simplified electronic potential, we find good agreement with calculations employing more refined potentials. [S1050-2947(97)07007-8]

PACS number(s): 79.20.-m

I. INTRODUCTION

In the past, considerable interest has been devoted to the detailed study of electronic processes that take place in ion-metal-surface interactions. On the experimental side, the emphasis has been on cases involving highly charged ions. A large number of sophisticated investigations have dealt with the formation of hollow-atom states by resonant electron capture and the observation of their decay by means of high-resolution Auger electron spectroscopy [1–3], with the formation of negative ions [4], with angular and charge state distributions of ions scattered from a single-crystal surface [5,6], and with the image charge attraction of ions in front of metal surfaces [7,8].

On the theoretical side, there is still a lack of manageable (time-dependent) dynamical theories taking into account both single-particle (excitation, resonant neutralization, and ionization) and many-particle effects (Auger deexcitation, Auger neutralization, plasmon excitation). Extreme difficulties with the formulation and implementation of such theories arise from the inherent complexity of the many-electron problem. One therefore has to resort to simpler models. Neglecting two-electron processes (which are supposed to be of minor importance at not too small ion-surface distances) and adopting a jellium description of the metal, a variety of theoretical studies have been undertaken both within the fixed-ion approximation and by approximately solving the time-dependent Schrödinger equation. Perturbative calculations have been performed by Gadzuk [9] and Remy [10], and more recently by Thumm and Briggs [11,12], Thumm [13,14], Wille [15–21], and Kürpick and Thumm [22]. Closed-form expressions for electron-transfer matrix elements as well as universal scaling properties of transition

rates were derived and analyzed by Wille [15,20] and by Kürpick and Thumm [22]. Nonperturbative approaches have been pursued by various groups using the self-energy concept [23,24], the time-dependent Newns-Anderson formalism [25,26], the coupled-angular-mode method [27–30], the complex-scaling method [31,32], a close-coupling method based on generalized Wannier functions [33], the stabilization method [34,35(a)], a multicenter Gaussian basis expansion method [36], a simplified close-coupling method [37], and a linear-combination-of-atomic-orbitals method with local-density many-body contributions [38].

Most of the nonperturbative *ab initio* methods applied so far are based on single-center expansions of the one-electron wave function, i.e., the wave function is expanded in terms of basis functions centered solely at the ion site. Hence the wave function is only poorly represented in the metal region, and the convergence of these expansions is very slow. In specific cases [32,34,35], basis sets with dimension exceeding 1000 have been used. Recently, the possibility to achieve better convergence by using a multicenter Gaussian expansion of the wave function has been examined [36].

In a pioneering paper by Burgdörfer *et al.* [23] the self-energy method used in this paper was introduced and applied to the interaction of $H(n=2)$ states with a gold surface at grazing incidence. The self-energy approach is based on a “two-center” expansion of the time-dependent electronic wave function, in which, in addition to a set of (bound) ion-centered basis functions, a set of functions describing the conduction band states of the metal is included. Neglecting the direct couplings between the conduction band states, one may reduce the full close-coupling problem associated with the two-center expansion [39,23,24] to a problem defined in the space of ionic basis functions only. The two-center char-

acter of the basis is retained, to some extent, in the complex (non-Hermitian) effective interaction acting in the ionic space, which embodies couplings between ionic and conduction band states. In the fixed-ion approximation, which we will adopt throughout, the (static) self-energy is defined [23,24] as the Laplace transform of the effective interaction. The self-energy determines the (real) energies and resonance widths as well as the resonance wave functions of “dressed” ionic states.

Since the work of Burgdörfer *et al.* [23], no systematic large-scale application of the self-energy method has been reported. Therefore a comprehensive study of this method appears timely, particularly in view of significantly improved computational resources and promising applications to chemisorption, surface diagnostics, and catalysis.

In this paper we evaluate the electronic self-energy of ions interacting with a metal surface within a model framework that, while being sufficiently realistic, allows calculations to be performed with reasonable effort. We employ a hydrogenic description of the ionic states along with the jellium approximation for the conduction band states. The classical image interactions are approximately taken into account. The emphasis in our study will be on the evaluation of the self-energy at different levels of approximation, starting with the first-order distortion of the ionic energy levels and going up to the full self-energy of the dressed ionic states. In doing so, we will be able to identify the effects that are brought in by the various couplings among the ionic basis states. We also consider the convergence properties of the self-energy method and compare our results to those obtained by other authors.

We believe that the results of our study are useful in several respects: (i) they demonstrate the feasibility of large-scale self-energy calculations; (ii) they supplement the results of other nonperturbative calculations; (iii) they provide insight into the way in which the individual interactions in the ion-metal system conspire to produce characteristic features of the resonance energies and widths; (iv) they form an appropriate starting point for the full time-dependent treatment of the ion-surface interaction within the coupled-state approach [40].

The present paper is organized as follows. A brief summary of the self-energy method is presented in Sec. II. In Sec. III we specify the model framework within which our calculations are performed and present some details of the explicit evaluation of various quantities. In Sec. IV the self-energy method is applied to the specific case of protons interacting with an aluminum surface, and a detailed analysis and discussion of our results is performed. Finally, Sec. V contains a summary of the paper as well as some concluding remarks. Throughout this paper, we use atomic units ($e = m_e = \hbar = 1$).

II. SELF-ENERGY METHOD

In this section we summarize the essential ingredients of the self-energy description of ion-surface interactions [23,24] and outline our general concept for evaluating the self-energy.

We start from the time-dependent Schrödinger equation for the total one-electron wave function $|\Psi(t)\rangle$,

$$i|\dot{\Psi}(t)\rangle = H(t)|\Psi(t)\rangle, \quad (1)$$

in which the Hamiltonian $H(t)$ is time dependent due to the motion of the ion along a prescribed classical trajectory (we adopt a reference frame in which the metal is at rest). The function $|\Psi(t)\rangle$ is expanded as

$$|\Psi(t)\rangle = \sum_{j=1}^N a_j(t)|\psi_j(t)\rangle + \int_{k \leq k_{\max}} d\vec{k} \rho(\vec{k}) b_{\vec{k}}(t) |\phi_{\vec{k}}\rangle, \quad (2)$$

where the basis functions $|\psi_j(t)\rangle$ are bound-state wave functions with energy ϵ_j centered at the ion site (the label j denotes collectively a set of single-particle quantum numbers), and N is finite. The basis functions $|\phi_{\vec{k}}\rangle$ are jellium wave functions corresponding to wave vector \vec{k} and energy $\epsilon_{\vec{k}}$, and $\rho(\vec{k})$ is the density of jellium states. We restrict the jellium basis to functions localized in the metal half space, so that the maximum wave number is given by $k_{\max} = \sqrt{2V_0}$, where V_0 denotes the bulk depth of the jellium potential.

By inserting expansion (2) into the Schrödinger equation (1) and projecting onto the basis functions, we obtain the set of close-coupling equations

$$i\dot{a}_j(t) = \sum_{j'} H_{jj'}(t) a_{j'}(t) + \int_{k' \leq k_{\max}} d\vec{k}' \rho(\vec{k}') H_{jk'}(t) b_{\vec{k}'}(t) - i \int_{k' \leq k_{\max}} d\vec{k}' \rho(\vec{k}') N_{jk'}(t) \dot{b}_{\vec{k}'}(t), \quad j=1, \dots, N \quad (3)$$

$$i\dot{b}_{\vec{k}}(t) = \sum_{j'} H_{\vec{k}j'}(t) a_{j'}(t) + \int_{k' \leq k_{\max}} d\vec{k}' \rho(\vec{k}') H_{\vec{k}\vec{k}'}(t) b_{\vec{k}'}(t) - i \sum_{j'} N_{\vec{k}j'}(t) \dot{a}_{j'}(t), \quad k \leq k_{\max}. \quad (4)$$

The matrix elements

$$H_{jj'}(t) = \langle \psi_j(t) | H(t) | \psi_{j'}(t) \rangle \equiv H_{jj'}^*(t), \quad (5)$$

$$H_{j\vec{k}}(t) = \langle \psi_j(t) | H(t) | \phi_{\vec{k}} \rangle \equiv H_{j\vec{k}}^*(t), \quad (6)$$

$$H_{\vec{k}\vec{k}'}(t) = \langle \phi_{\vec{k}} | H(t) | \phi_{\vec{k}'} \rangle \equiv H_{\vec{k}\vec{k}'}^*(t) \quad (7)$$

describe direct couplings in the ionic space, couplings between ionic and jellium states, and direct couplings among the jellium states, respectively (we have ignored velocity-dependent dynamic couplings [39] as well as contributions from translational factors [23,24,13], which are evidently irrelevant for our purpose). The nonorthogonality of ionic and jellium basis functions is taken into account through the overlap matrix elements

$$N_{j\vec{k}}(t) = \langle \psi_j(t) | \phi_{\vec{k}} \rangle \equiv N_{j\vec{k}}^*(t). \quad (8)$$

The fixed-ion approximation corresponds to the static limit in which the ion is at rest at a distance D in front of the surface. Accordingly, the Hamiltonian H is independent of time and depends only parametrically on D (in the following,

we will indicate the D dependence of the coupling matrix elements and other quantities only when indispensable). In this case, the set of close-coupling equations (3) and (4) can be converted, by means of a Laplace transformation in the variable s , into a system of algebraic equations for the transformed expansion coefficients $\tilde{a}_j(s)$ and $\tilde{b}_k(s)$. If the direct couplings $H_{kk'}$ among the jellium states are neglected, the coefficients $\tilde{b}_k(s)$ can be eliminated from the algebraic system. The resulting system for the ionic coefficients $\tilde{a}_j(s)$, corresponding to initial conditions where the Fermi sea of metal electrons is completely filled and the ionic levels are unoccupied, reads

$$\sum_{j'} [is\delta_{jj'} - \mathcal{S}_{jj'}(s)] \tilde{a}_{j'}(s) = i \int_{k \leq k_F} d\bar{k} \rho(\bar{k}) \frac{W_{jk}}{is - \epsilon_{\bar{k}}}, \quad (9)$$

where k_F is the Fermi momentum of the metal, and $\mathcal{S}(s)$ is the complex (static) self-energy. The self-energy describes the effective interaction that governs the dynamics in the ionic space in the presence of couplings to the jellium states. When expressing s in terms of the real energy variable ω by $s = -i\omega + \eta$, the matrix elements of $\mathcal{S}(\omega)$ are given by

$$\begin{aligned} \mathcal{S}_{jj'}(\omega) = & \epsilon_j \delta_{jj'} + F_{jj'} + P \int_{k \leq k_{\max}} d\bar{k} \rho(\bar{k}) \\ & \times \frac{[(\epsilon_{\bar{k}} - \omega) N_{j\bar{k}} + W_{j\bar{k}}][(\epsilon_{\bar{k}} - \omega) N_{j'\bar{k}}^* + W_{j'\bar{k}}^*]}{\omega - \epsilon_{\bar{k}}} \\ & - i\pi \int_{k \leq k_{\max}} d\bar{k} \rho(\bar{k}) W_{j\bar{k}} W_{j'\bar{k}}^* \delta(\omega - \epsilon_{\bar{k}}), \quad (10) \end{aligned}$$

where P denotes the principal part and η is an infinitesimal guaranteeing that (Siegert) resonance boundary conditions are fulfilled. The initial-channel transfer matrix elements $W_{j\bar{k}}$ and the final-channel distortion matrix elements $F_{jj'}$ are defined as [22]

$$W_{j\bar{k}} = \langle \psi_j | V_i | \phi_{\bar{k}} \rangle \quad (11)$$

and

$$F_{jj'} = \langle \psi_j | V_f | \psi_{j'} \rangle. \quad (12)$$

The principal-part term in Eq. (10) describes indirect couplings between ionic states due to virtual transitions into the conduction band (and back to the ion), while the term proportional to $i\pi$ ("width term") describes real transitions into the conduction band and gives rise to the resonance broadening of the dressed ionic levels.

The specific form in which Eqs. (9) and (10) are written corresponds to the channel decomposition

$$H = H_i + V_i \quad (13)$$

of the total Hamiltonian H in the coupling matrix elements H_{jk} , and to the channel decomposition

$$H = H_f + V_f \quad (14)$$

in the matrix elements $H_{jj'}$. The Hamiltonians H_i and H_f , respectively, define the unperturbed initial jellium states and final ionic states, and V_i and V_f are the associated channel perturbations (to be specified in Sec. III).

The complex eigenvalues $\tilde{\omega}_\mu$ of the self-energy matrix $\mathcal{S}(\omega)$ determine the (real) energies E_μ and the resonance widths Γ_μ of dressed ionic states $|\chi_\mu\rangle$ through

$$E_\mu = \text{Re } \tilde{\omega}_\mu, \quad (15)$$

$$\Gamma_\mu = -2 \text{Im } \tilde{\omega}_\mu. \quad (16)$$

The associated eigenvectors constitute the resonance wave functions of the states $|\chi_\mu\rangle$. The label μ collectively denotes the conserved quantum numbers that characterize the self-energy matrix and an index that counts the eigenvalues for given quantum numbers. Instead of solving the (nonlinear) eigenvalue problem for $\mathcal{S}(\omega)$, we evaluate the matrix elements $\mathcal{S}_{jj'}(\omega)$ at the position [13]

$$\omega = \frac{\epsilon_j + \epsilon_{j'}}{2} \equiv \omega_{jj'} \quad (17)$$

(this formula generalizes the usual Wigner-Weisskopf approximation [24] to the case of nondegenerate ionic levels) and subsequently diagonalize the (fixed) matrix $\mathcal{S}(\{\omega_{jj'}\})$.

III. MODEL FRAMEWORK

We now turn to the specific model assumptions that enter our calculations and present some details regarding the numerical evaluation of the coupling matrix elements and the self-energy. We choose electronic coordinates $\vec{r} \equiv (x, y, z)$ such that the (x, y) plane coincides with the jellium edge of the metal and the z axis (with the ion center located on it) points towards the vacuum. The image reference plane is assumed to coincide with the jellium edge at $z=0$.

The underlying total one-electron Hamiltonian H is taken in the form

$$H = T + V_J + V_C^> + V_e^{(i)} + V_C^{(i)}, \quad (18)$$

where T is the kinetic energy. For the jellium potential V_J , we assume a simple, step-functional form,

$$V_J(z) = -V_0 \Theta(-z). \quad (19)$$

The potential $V_C^>$ is the potential of the ion core, cut off at the surface in order to allow for the complete screening of the core potential inside the metal. In the hydrogenic approximation which we adopt here, we have

$$V_C^>(\vec{r}; D) = V_C(\vec{r}; D) \Theta(z), \quad (20)$$

where

$$V_C(\vec{r}; D) = \frac{-Z}{|\vec{r} - D \hat{e}_z|} \quad (21)$$

is the full Coulomb potential of the projectile core of effective charge number Z . The potentials

$$V_e^{(i)}(z) = -\frac{1}{4z} \Theta(z) \quad (22)$$

and

$$V_C^{(i)}(\vec{r}; D) = \frac{Z}{|\vec{r} + D\hat{e}_z|} \Theta(z) \quad (23)$$

are the classical image potentials induced by the active electron and by the ion core, respectively.

The channel Hamiltonians H_i and H_f defining the unperturbed initial and final states [cf. Eqs. (13) and (14)] are

$$H_i = T + V_J, \quad (24)$$

with analytical eigenfunctions $|\phi_k\rangle$ [15,22] and energies $\epsilon_k = \vec{k}^2/2 - V_0$, and

$$H_f = T + V_C. \quad (25)$$

For the (hydrogenic) eigenfunctions of H_f , we adopt the spherical representation $|\psi_{nlm}\rangle$. From Eqs. (13), (14), and (18), the channel perturbations V_i and V_f are now identified as

$$V_i = V_C^> + V_e^{(i)} + V_C^{(i)} \quad (26)$$

and

$$V_f = V_J - V_C^< + V_e^{(i)} + V_C^{(i)}, \quad (27)$$

where

$$V_C^< = V_C - V_C^> \quad (28)$$

is the ‘‘metal part’’ of the core potential [note that $V_C^<$ occurs in Eq. (27) with a minus sign in front].

The coupling matrix elements W_{jk} and $F_{jj'}$ [cf. Eqs. (11) and (12)] are hard to deal with if the channel perturbations V_i and V_f are kept in full. In order to keep the numerical effort at a manageable level, we approximate the core image potential $V_C^{(i)}$ by its values on the z axis [13],

$$V_C^{(i)}(\vec{r}; D) \approx \frac{Z}{|z + D|} \Theta(z) \equiv V_C^{(i)}(z; D). \quad (29)$$

Through this approximation, the repulsive character of the core image potential is enhanced and, accordingly, the energies of the dressed ionic states will be raised and the resonance widths lowered. However, the inaccuracies decrease with increasing ion-surface distance D and are estimated to be very small for $D > \langle r \rangle_n$, where $\langle r \rangle_n \equiv n^2/Z$ is the (classical) mean radius of the projectile n manifold (for a quantitative assessment see Sec. IV A below).

In order to remove the unphysical singularity of the electron self-image potential $V_e^{(i)}$ at $z=0$, we set [13]

$$V_e^{(i)}(z) + V_C^{(i)}(z; D) = 0, \quad z < z_0 \quad (30)$$

where z_0 is determined from the condition

$$V_e^{(i)}(z_0) + V_C^{(i)}(z_0; D) = -V_0, \quad (31)$$

i.e.,

$$z_0 = \frac{1}{2} \left(\sqrt{D_0^2 + \frac{D}{V_0}} - D_0 \right), \quad (32)$$

where

$$D_0 = D + \frac{Z}{V_0} - \frac{1}{4V_0}. \quad (33)$$

For our explicit calculations, we now write the final-channel perturbation V_f as

$$V_f(z) = \begin{cases} -V_0 - V_C^<, & z < z_0 \\ V_e^{(i)}(z) + V_C^{(i)}(z; D), & z \geq z_0 \end{cases} \quad (34)$$

where we have shifted the jellium edge to $z=z_0$, so that the jellium potential is smoothly joining the total image potential (for the p -Al case, z_0 varies from 0 to 0.43 a.u. when D varies from 0 to ∞). The term $V_C^<$ has a sizable effect only on the $1s$ state at small ion-surface distances. Except for the $1s$ case, we have therefore disregarded in our calculations the contribution of this term.

In the initial-channel perturbation V_i , we keep the Coulomb potential only,

$$V_i = V_C^>, \quad (35)$$

i.e., we neglect the image potentials completely. While the evaluation of individual matrix elements W_{jk} including the full perturbation V_i is easily accomplished by means of the technique developed in Refs. [15,22], it turns out that \vec{k} integrations encountered in the self-energy matrix (10) render a calculation with the full V_i prohibitively time-consuming. The approximation (35) appears to be the most severe approximation we have to introduce in our calculations. Qualitatively, the behavior of the ‘‘transfer matrix element’’ W_{jk} is dominated by the ‘‘classical-threshold distance’’ corresponding to the potential V_i [15,18]. Simple estimates [24] show that the neglect of the image interaction in V_i results in a decrease of the threshold distance if $Z < 2$, and in an increase if $Z > 2$. Correspondingly, the overall magnitude of the approximate W_{jk} is expected to be smaller than that of the full W_{jk} if $Z < 2$, and larger if $Z > 2$.

Since the ion-surface interaction is axially symmetric about the surface normal, the magnetic quantum number m is a conserved quantum number throughout, so that the self-energy matrix can be considered separately in the subspaces corresponding to different m values.

In the evaluation of the coupling matrix elements $F_{nlm, n'l'm}$ with the perturbation (34) and hydrogenic wave functions $|\psi_{nlm}\rangle$, we employ the analytical reduction of the three-dimensional integration to a one-dimensional integration given in Ref. [22]. The remaining integration is easily performed numerically. The coupling matrix elements $W_{nlm, \vec{k}}$ with the perturbation (35) as well as the overlap matrix elements $N_{nlm, \vec{k}}$ are evaluated using the closed-form expressions of Ref. [15]. For the actual computation of these expressions, we have developed a highly optimized com-

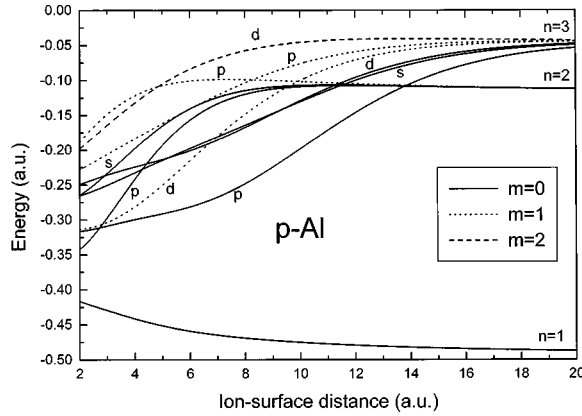


FIG. 1. First-order distorted energies calculated from Eq. (37) for all states with $n \leq 3$.

puter code, thereby enabling the efficient and accurate evaluation of the self-energy matrix in a large space of hydrogenic states.

The \vec{k} integrations in the principal-part term and in the width term of the self-energy matrix (10) are evaluated with the density of states taken equal to the free-electron-gas density, $\rho(\vec{k}) = (2\pi)^{-3}$ (for a given electronic spin direction). Due to axial symmetry, the azimuthal integration is trivial. In the numerical evaluation of the remaining two-dimensional integral for the principal-part term, special precautions are taken to avoid unduly large errors that might arise from the singularity in the integrand. The width term in Eq. (10) (also referred to as on-shell contribution) can be reduced to a one-dimensional integral by exploiting the energy-conserving δ function.

IV. SELF-ENERGY CALCULATIONS

We now apply the self-energy method, within the model framework outlined above, to the calculation of energies and resonance widths of dressed ionic states. Specifically, we consider the case of protons ($Z=1$) interacting with an aluminum surface ($V_0=0.585$ a.u.). This example is chosen in order to enable the comparison of our results to those of previous calculations by other authors.

A. Direct couplings between unperturbed projectile states

In order to examine the effect of the different terms in the self-energy matrix (10), we first consider direct couplings within the ionic space given by the energy matrix \mathcal{F} with elements

$$\mathcal{F}_{jj'} = \epsilon_j \delta_{jj'} + F_{jj'} . \quad (36)$$

The first-order distorted energy corresponding to the unperturbed state $|\psi_{nlm}\rangle$ is then obtained as

$$E_{nlm} = \mathcal{F}_{nlm,nlm} \equiv \epsilon_n + F_{nlm,nlm} . \quad (37)$$

In Fig. 1 we show the first-order distorted energies for the n manifolds up to $n=3$ as a function of the ion-surface distance D . For D larger than the ‘‘scaling distance’’ $2\langle r \rangle_n \equiv 2n^2$ [22], the energy curves follow the $1/4D$ dependence anticipated from the leading term in the $1/D$ expansion

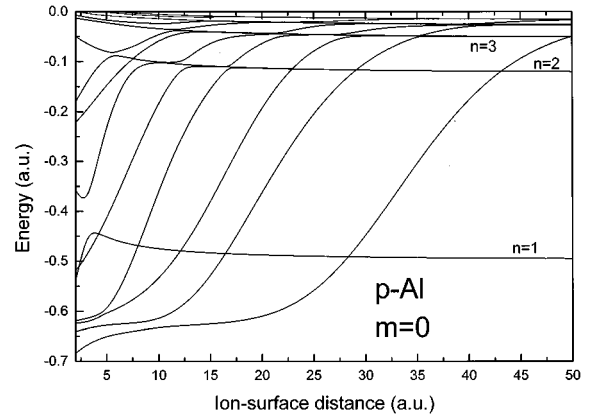


FIG. 2. Converged energies of all ($m=0$) states emerging from the unperturbed manifolds up to $n=4$, obtained as eigenvalues of the direct-coupling matrix \mathcal{F} [Eq. (36)]. States up to $n=6$ have been included in the ionic basis space.

of the image interaction $V_e^{(i)} + V_C^{(i)}$ [30,32]. When D falls below $2n^2$, the energies are progressively lowered due to the effect of the attractive jellium potential. As the overlap of the ionic orbitals with the metal is larger for larger n , this effect increases with increasing n and leads to crossings of the levels emerging from high- n shells with lower- n levels. While the distorted energies exhibit a sizable dependence on the orbital angular momentum l (at fixed n and m), there is an even stronger dependence on the magnetic quantum number m (at fixed n and l), with the low- m states being affected strongest. The m dependence reflects the strong change in shape which the ionic wave function undergoes with changing m , and the associated change in the overlap of the ionic wave function with the jellium potential [22].

In a second step, the energies $E_{\mu m}$ are determined as eigenvalues of the matrix \mathcal{F} (the label μ attached to $E_{\mu m}$ counts the eigenvalues for given m). In Fig. 2 we display energies as a function of D for all ($m=0$) states that merge asymptotically into unperturbed states with $n \leq 4$. In the diagonalization of \mathcal{F} , unperturbed states with $n \leq 6$ were taken into account to guarantee convergence of the displayed energies (see Sec. IV D). The pattern shown by the energy curves is characterized by a series of levels which, when followed to smaller distances, tend to become lowered, in some cases below the bottom of the conduction band. The strong level shift arises from large off-diagonal couplings in $\mathcal{F}_{jj'}$ in Eq. (36).

In order to investigate the approximation we made by using Eq. (29) for the nuclear image potential and by employing the step-function potential for the jellium surface, we calculated final-channel matrix elements (12) using both the more refined Jennings potential [41] for the surface (which includes the electronic self-image) and the full two-dimensional nuclear image potential according to Eq. (23). As an example Fig. 3 shows the diagonal final-channel matrix elements for the projectile $2s, 2p_1$, $3s, 3d_2$, and $4s, 4f_3$ states for both (i) the step-function potential and the simplified nuclear image potential (29) used in all our calculations and (ii) the more refined Jennings potential and nuclear image potential (23). As expected, the full nuclear image potential is less repulsive than our approximate nuclear image

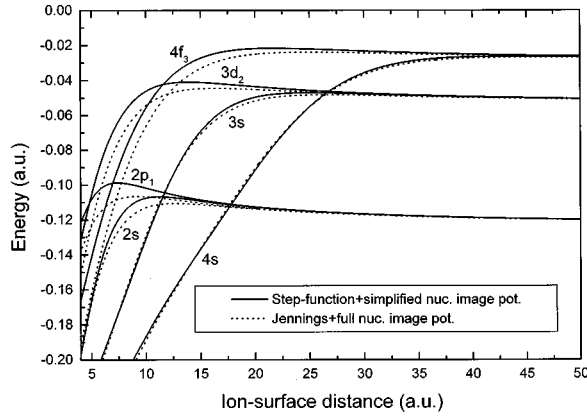


FIG. 3. Diagonal matrix elements for the first-order distorted energies for the one-dimensional potential [see Eq. (34)] (full line) and the potential built up by the Jennings potential [41] and the full nuclear image potential according to Eq. (23) (dotted line) for the $2s$, $2p_1$, $3s$, $3d_2$, and $4s$, $4f_3$ states.

potential which leads to a weaker energetic upward shift of the states. As can be seen the ($m=l$) states ($2p_1, 3d_2, 4f_3$) show the largest discrepancies between the two potentials. This can be easily understood as these states have a charge density which is aligned almost parallel to the surface and therefore strongly experiences the difference in the two nuclear image potentials used. The overall maximum energetic deviation for all cases shown is of the order of 0.01 a.u. ($2p_1$) and tends to become smaller for higher n -quantum numbers.

B. Diagonal elements of the self-energy matrix

Turning now to the full self-energy, we consider energies E_{nlm} and resonance widths Γ_{nlm} calculated from the diagonal elements of the self-energy matrix. The widths Γ_{nlm} (or, equivalently, the transition rates for resonant electron transfer) have been studied previously [13,16,17] within the model framework that is used in the present work.

In Fig. 4 energies E_{nlm} are shown as a function of D for the n manifolds up to $n=3$. The energy curves start to deviate from the curves of Fig. 1 when D drops below the classical-threshold distance $2n^2$, below which the magnitude

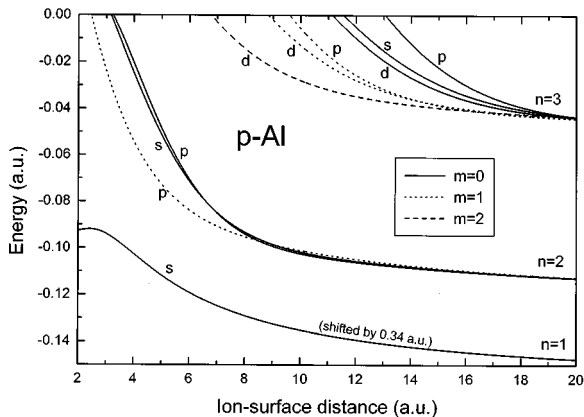


FIG. 4. Diagonal elements of the self-energy for all states with $n \leq 3$. We shifted the ($n=1$) energy by 0.34 a.u.

of the matrix elements W_{jk}^- and N_{jk}^- , and hence of the principal-part term in the self-energy, begins to rise steeply [15]. In marked contrast to the behavior of the perturbative energies of Fig. 1, all curves in Fig. 4, except the $1s$ curve, continue to increase monotonically down to very small D values. This behavior can be qualitatively understood by considering the diagonal elements of the principal-part term in Eq. (10). The numerator in the integrand is positive throughout, while the denominator is negative if $\epsilon_k^- > \epsilon_j$, and positive if $\epsilon_k^- < \epsilon_j$. Hence, when ϵ_k^- varies in the range $-V_0 \leq \epsilon_k^- \leq 0$, the integrand is essentially negative for ionic states with $\epsilon_j \approx -V_0$, and essentially positive for states with $|\epsilon_j| \ll V_0$. For our specific example, we therefore expect the $1s$ energy at small distances to be lowered by the principal-part term, and all other energies to be increased.

The effect of the principal-part term on the diagonal elements of the self-energy for $n > 1$ can be viewed as being equivalent to that of an effective potential which is strongly repulsive at small ion-surface distances. The surprising result is that this effective potential is strong enough to overcompensate completely the lowering of the levels caused by the attractive jellium potential.

We note that the strong m dependence of the principal-part contribution to the diagonal elements of the self-energy tends to reverse, in comparison with the first-order distorted energies, the order of the different m levels emerging from a hydrogenic n manifold. The $2p_1$ level, for example, is well below the $2s$ and $2p_0$ levels in Fig. 4, while the opposite holds for the corresponding levels in Fig. 1. It is also worth mentioning that the splitting of the diabatic self-energies at large distances is much smaller than that of the corresponding first-order distorted energies of Fig. 1. This feature appears to be an immediate consequence of the potential barrier that is effectively built up by the principal-part term.

C. Eigenvalues of the full self-energy matrix

In this subsection we present and analyze energies $E_{\mu m}$ and resonance widths $\Gamma_{\mu m}$ determined from the eigenvalues of the full self-energy matrix according to Eqs. (15) and (16), and perform a detailed comparison to the results obtained by other authors. Since these energies and widths are obtained by diagonalizing a non-Hermitian matrix the Wigner-von Neumann noncrossing rule does not apply and levels of the same symmetry may cross. To extract the physically relevant levels, i.e., the energetic path an electron would follow at finite velocity, we diabatically follow the levels so as to preserve the character of the associated wave function as a function of the ion-surface distance. This can be easily achieved by calculating the overlap matrix between all states of adjacent ion-surface distances and by connecting energies and widths of states with maximum overlap. The procedure gives smooth curves for energies and widths.

In Fig. 5, we display energy curves for the ($m=0$) states emerging from the unperturbed ($n=1, \dots, 4$) manifolds, by including n manifolds up to $n=6$ in the basis set. There is a striking qualitative difference between the curves of Fig. 5 and those of Fig. 2 for the energies including the direct couplings only. Except for the asymptotic ($n=1$) state, all curves in Fig. 5 continue to rise monotonically when D falls

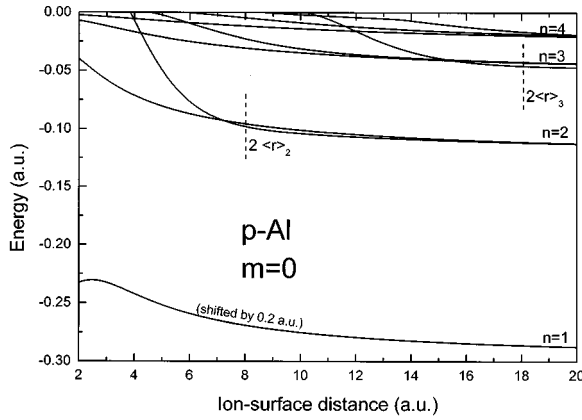


FIG. 5. Converged eigenvalues of the full self-energy matrix of all ($m=0$) states emerging from the unperturbed manifolds up to $n=4$. States up to $n=6$ have been included in the ionic basis space. The vertical dashed bars indicate the position of the threshold distances $2\langle r \rangle_n = 2n^2$ (see text).

below the threshold distance $2n^2$, and there are no remnants of the strongly lowered levels appearing in Fig. 2. This shows that the indirect couplings via the conduction band states, which we have found to have pronounced influence on the diagonal elements of the self-energy, prevail also in the full self-energy.

Comparing the results of Fig. 5 to the diagonal elements of the self-energy shown in Fig. 4, we observe different splitting patterns for levels emerging from one and the same n manifold at distances below the threshold distance $2n^2$. The levels emerging from the asymptotic ($n=2$) manifold in Fig. 5, for example, are much stronger split than their ‘‘parent levels’’ $2s$ and $2p_0$ in Fig. 4. This difference reflects the hybridization of hydrogenic orbitals with opposite parity that is caused mainly by the image potentials [31,30,32] (a more detailed discussion of hybridization properties of dressed ionic states will be presented in Sec. IV E).

In order to gain more insight into the interplay of the different couplings acting in the ion-metal system, we show in Fig. 6 energy curves calculated by keeping the principal-part term as the only term in the self-energy matrix as well as by keeping the principal-part together with the width term. As the image potentials contained in the final-channel perturbation V_f are now neglected, the asymptotic $1/4D$ behavior seen in Fig. 5 is absent in the curves of Fig. 6, and all curves, except the ($n=1$) state, display a flat behavior beyond the threshold distance $2n^2$. There is, however, a strong splitting of the levels emerging from a single n manifold. This shows explicitly that the corresponding splitting seen in Fig. 5 is, to a large extent, driven by the indirect couplings via the conduction band. The effect of the width term in the self-energy matrix on the energies is seen from Fig. 6 to be very small.

The energy of the state asymptotically merging into the $1s$ state is contrasted in Fig. 7 with the results of other non-perturbative calculations. At large and intermediate distances, our results agree well with the coupled-angular-mode results of Borisov *et al.* [27] and the stabilization-method results by Deutscher *et al.* [35], while a systematic deviation remains with the complex-scaling results of Nordlander and

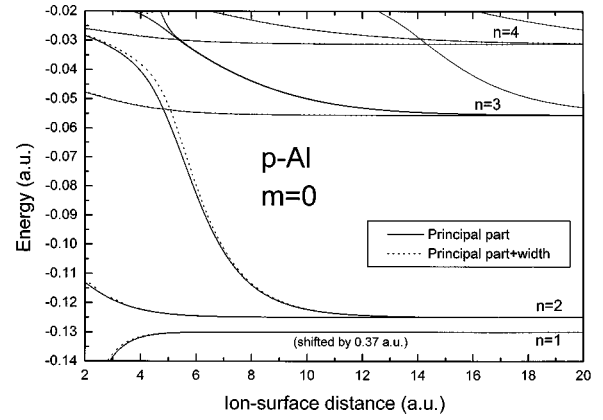


FIG. 6. Same as Fig. 5, but with the direct-coupling terms $F_{jj'}$ in the self-energy matrix (10) neglected (dashed curves). The full curves correspond to a calculation in which, moreover, the imaginary width term has been disregarded, i.e., in which only the principal-part term has been kept.

Tully [31]. Similar to our calculation the results of Deutscher *et al.* [35] using the stabilization method give a local maximum in the ($n=1$) energy curve at $D \approx 3.5$ a.u. Our energy curve shows a maximum at $D=2.5$ a.u. We note that the qualitative behavior of our ($n=1$) energy at small distances is decisively influenced by the V_f term (34) in the total self-energy (10). To illustrate this effect we have drawn in Fig. 7 the contribution from the $1s$ diagonal matrix element of the final channel potential according to Eq. (12) (labeled as V_f only). At distances D larger than 4 a.u. it coincides with the result of the full self-energy calculation. However, for smaller ion-surface distances the principal-part term in the full self-energy tends to enhance the binding energy of the ($n=1$) resonance state.

The resonance width of the asymptotic ($n=1$) state is compared in Fig. 8 to other nonperturbative calculations by Nordlander and Tully [31], Borisov *et al.* [27], where results are shown for both a classical image potential and a smeared surface charge, Deutscher *et al.* [35], and perturbative results by Wille [17]. The fairly large discrepancies between the different theoretical approaches apparently reflect the differ-

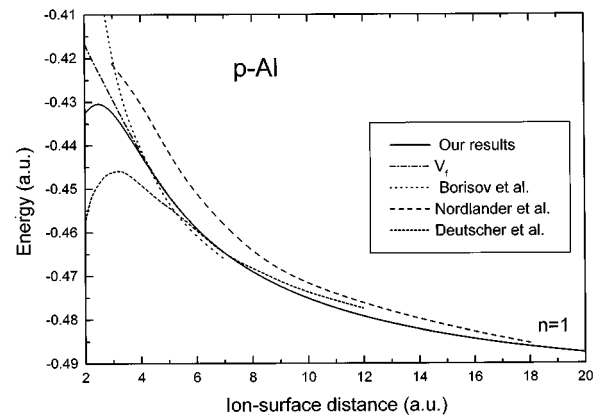


FIG. 7. Comparison of the energy of the asymptotic ($n=1$) state, calculated from the full self-energy matrix (10), with the non-perturbative results of Nordlander and Tully [31], Deutscher *et al.* [35], and Borisov *et al.* [27].

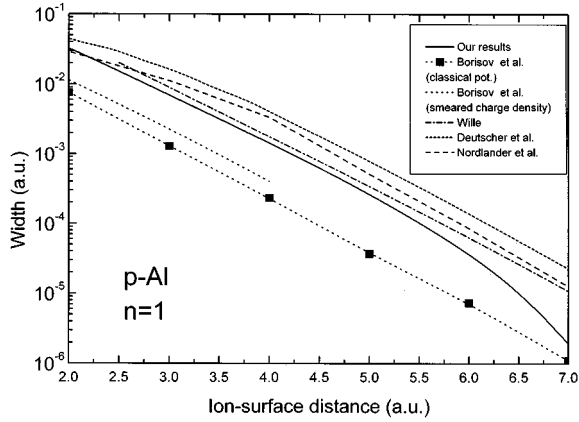


FIG. 8. Comparison of the width of the asymptotic ($n=1$) state, calculated from the full self-energy matrix (10), to the nonperturbative results of Nordlander and Tully [31], Borisov *et al.* [27], and Deutscher *et al.* [35].

ent choices of the surface potential and the strong sensitivity of the width to details of the potential, in particular for strongly bound states.

In Figs. 9 and 10, the energies emerging from the ($n=2$; $m=0$) and ($n=3$; $m=0,1$) manifolds are shown in comparison with results of Nordlander and Tully [31] and of Borisov *et al.* [27] as well as with the multicenter calculation of Martín and Politis [36] and very recent results by Deutscher *et al.* [35(b)]. There is good agreement of our results with the other calculations, in particular with those of Nordlander and Tully. Hence details of the electronic potential appear to have small influence on the energies.

In Figs. 11 and 12, the resonance widths corresponding to the energies of Figs. 9 and 10 [note that we have used the same symbols (a, b, \dots) to designate energies and widths in Figs. 9–12] are compared to the nonperturbative results of Nordlander and Tully [31], Borisov *et al.* [27], Deutscher *et al.* [35(b)], as well as to the first-order calculation of Wille [17] in which the parabolic (Stark) representation of the hy-

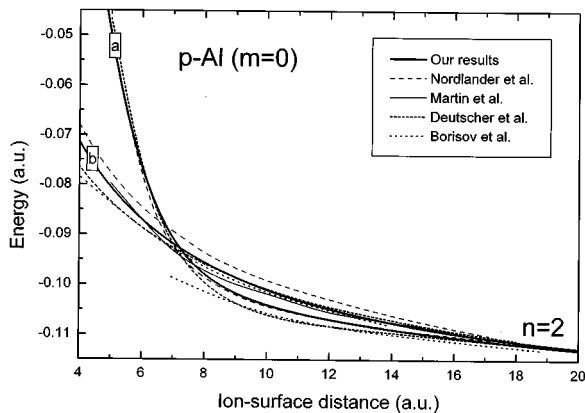


FIG. 9. Comparison of the resonance energies for ($m=0$) states emerging from the unperturbed ($n=2$) manifold, calculated from the full self-energy matrix (10), to the nonperturbative results of Nordlander and Tully [31] Borisov *et al.* [27], Martín and Politis [36], and Deutscher *et al.* [35(b)]. The letters a and b refer to the corresponding widths in Fig. 11.

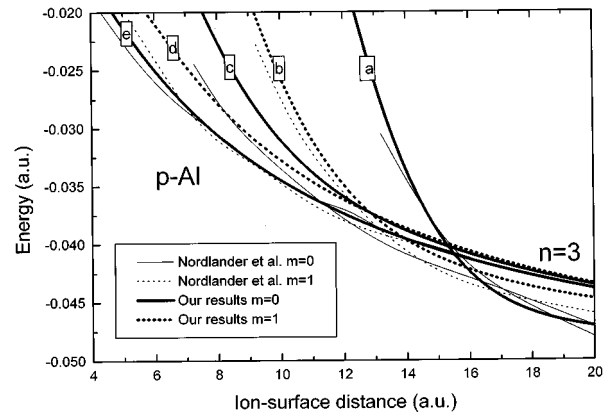


FIG. 10. Comparison of the resonance energies for all ($m=0$) and ($m=1$) states emerging from the unperturbed ($n=3$) manifold, calculated from the full self-energy matrix (10), to the nonperturbative results of Nordlander and Tully [31]. The letters a – e refer to the corresponding widths in Fig. 12.

drogenic wave functions has been used to simulate orbital hybridization.

Our $n=2$ results in Fig. 11, while being in close overall agreement with the other calculations tend to be consistently smaller than the other nonperturbative results by a factor of 1.5 to 2. Qualitatively, we ascribe these discrepancies to (i) our approximation (29) for the core image potential and (ii) our use of a jellium potential with a sharp step instead of the smoothed potential used in Refs. [31,27,35]. The $n=3$ results in Fig. 12 exhibit the same trend as the $n=2$ results, with widths now being generally smaller than the nonperturbative widths of Nordlander and Tully [31]. However, this rule does not hold for the state with the smallest width which tends to be bigger than the results by Nordlander for large ion-surface distances and smaller for distances below $D = 12$ a.u.

D. Convergence properties

In the full self-energy calculations presented above, we have used basis spaces of fixed dimension N_{basis} , and we

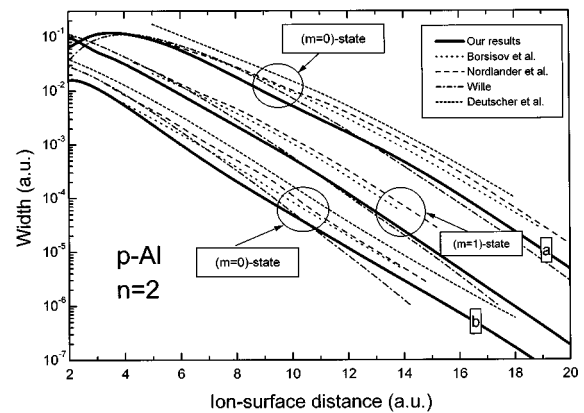


FIG. 11. Comparison of the resonance widths for all states emerging from the unperturbed ($n=2$) manifold, calculated from the full self-energy matrix (10), to the nonperturbative results of Nordlander and Tully [31], Borisov *et al.* [27], Deutscher *et al.* [35], and to the first-order calculation with hydrogenic states in parabolic representation of Wille [17].

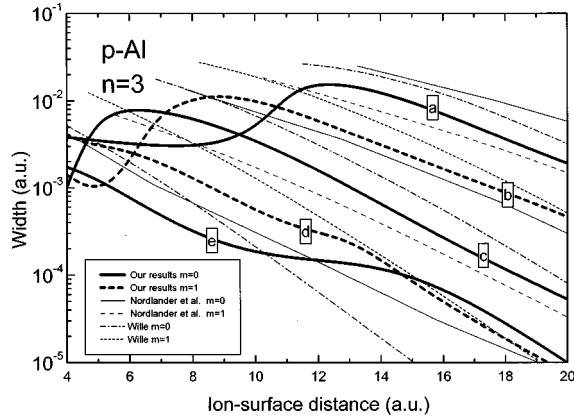


FIG. 12. Comparison of the resonance widths for all states emerging from the unperturbed ($n=3$) manifold, calculated from the full self-energy matrix (10), to the nonperturbative results of Nordlander and Tully [31], and to the first-order calculation with hydrogenic states in parabolic representation of Wille [17].

have not dwelt upon the question to what extent the results are converged, i.e., to what extent the energies and widths are changing when N_{basis} is changed. We now turn to a discussion of this issue. As a representative case, we consider the ($m=0$) states where we have so far used the 21 lowest hydrogen states ($n=1, \dots, 6$; $l=0, \dots, n-1$) as basis states.

Taking as example a particular ($m=0$) resonance state which asymptotically merges into the ($n=4$) manifold, Figs. 13(a) and 13(b) show the convergence of the energy and width for an increasing number N_{basis} of bound hydrogen basis ($m=0$) orbitals. The inset in Fig. 13(a) shows the chosen ($n=4$) state as dotted line among all other resonance states of the ($n=2, \dots, 6$; $m=0$) manifolds. As can be seen, major changes in the energy and width occur between $N_{\text{basis}}=10$ and $N_{\text{basis}}=15$ while almost no change is observed between $N_{\text{basis}}=15$ and $N_{\text{basis}}=21$. A similar rapid convergence is observed for all ($n \leq 5$) manifolds. The asymptotic ($n=6$) manifold would require the inclusion of higher basis orbitals (with $n \leq 7$) to become converged.

Summarizing the evidence obtained from these examples, we conclude that the ($m=0$) results of the self-energy cal-

culations presented above are well converged for $n \leq 5$ in the chosen ionic basis. Similar convergence is reached for higher m -quantum numbers. The remaining inaccuracies caused by truncating the ionic basis space are considerably smaller than those introduced by uncertainties in the electronic potentials. This also supports our intuitive expectation that, with respect to the target-centered part of the basis, the technically difficult inclusion of positive energy continuum states is of little or no relevance. Since these target-centered continuum functions (here: jellium functions of positive energy) overlap with projectile-centered hydrogenic orbitals, our convergence study has to some extent probed the influence of the part of Hilbert space that is represented by the target continuum. As a general rule we found, even for small ion-surface distances, that a given n manifold is converged if the adjacent ($n-1$) and ($n+1$) manifolds are included in the close-coupling expansion.

Further evidence for sufficient completeness of our basis is provided by the good agreement between our calculation and the results of Nordlander and Tully [31], Borisov *et al.* [27], and Deutscher *et al.* [35A] (see Sec. IV C). The complex rotation technique in Ref. [31] includes part of the continuum basis through complex rotated and thus square integrable continuum states.

In conjunction with the discussion of the convergence properties of our self-energy calculations, a comment is in order on the computational work that is required in the various steps of the calculations. Within our model framework, the basic distortion and transfer matrix elements are essentially reduced to closed-form expressions [15,22] which allow a fast and accurate evaluation of individual matrix elements even for ionic states with very high quantum numbers ($n=20$ and larger). The most time-consuming step in our calculations is the evaluation of the \vec{k} integrals in the principal-part term of the self-energy matrix. Given the self-energy matrix, the effort spent in its diagonalization is negligibly small in comparison with the effort spent in other methods (complex-scaling method, stabilization method) to diagonalize the full Hamiltonian matrix within a very large basis [35]. This advantage which results from the fact that we effectively use a two-center basis to describe the electronic wave function, is partially deteriorated by the consid-

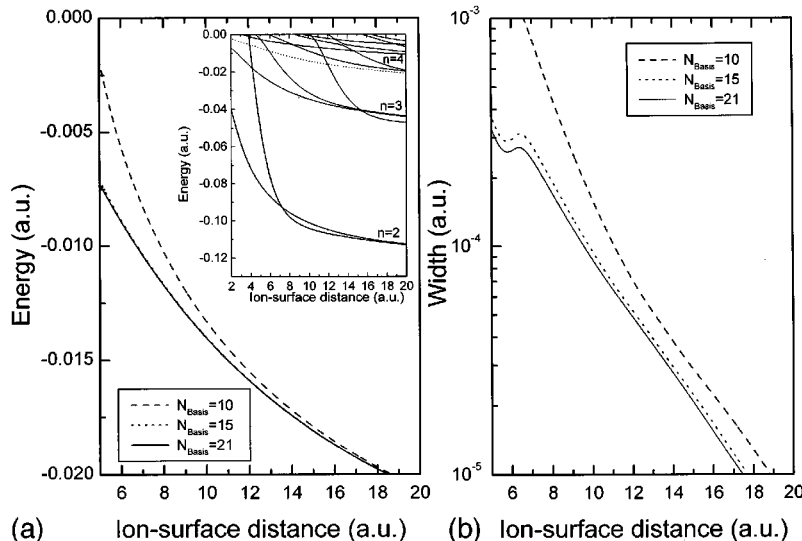


FIG. 13. Resonance energy (a) and width (b) of an ($m=0$) state asymptotically merging into the ($n=4$) manifold obtained for various sizes of the basis set. The inset shows the chosen resonance state among all other ($m=0$) states of the ($n=2$) to ($n=6$) manifolds as a dotted line.

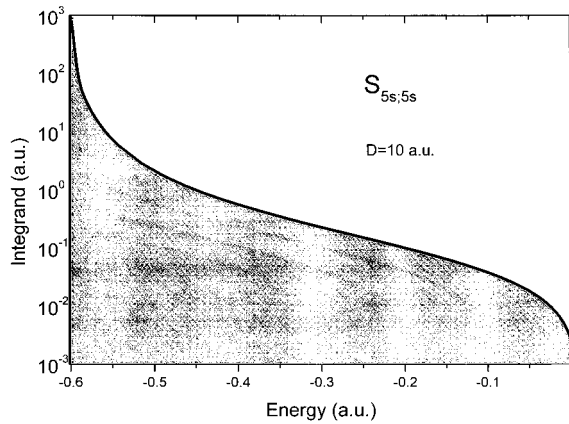


FIG. 14. Numerator of the integrand of the principal part in the full self-energy matrix element $S_{5s,5s}$ [Eq. (10)] at $D=10$ a.u.

erably larger computational work spent to evaluate the effective interaction (self-energy).

Besides the convergence with respect to the bound ionic states, we studied the influence of the upper integration limit k_{\max} [see Eq. (2)] in the jellium basis by investigating the structure of the integrand in the principal part of the self-energy matrix (10). Both diagonal and off-diagonal matrix elements show a very pronounced maximum in the integrand

near the bottom of the conduction band (the integrand is 0 at $k=0$). This maximum results from the very long wavelength of the corresponding metal part of the jellium states which avoids cancellation effects in the overlap and Coulomb initial-channel transfer matrix elements. Figure 14 shows a typical numerator of the integrand for the principal part of the $S_{5s,5s}$ matrix element at $D=10$ a.u. From the figure it is obvious that increasing the upper integration limit (beyond the ionization threshold) would not significantly alter the influence of the principal part on the total self-energy matrix.

E. ORBITAL HYBRIDIZATION

Having studied so far the energies and widths of dressed ionic states, we now briefly discuss the wave functions associated with these states. The dressed wave functions describe hybridized orbitals that are formed in front of the metal surface. Previous studies [29,30–32,34,35] have shown that at large ion-surface distances orbital hybridization gives rise to a pattern for the energies and wave functions that is in close resemblance with the pattern characteristic of Stark states (i.e., of hydrogenic states described by wave functions in parabolic representation). Here, we examine hybridized orbitals at small distances where strong mixing of different hydrogenic n shells occurs.

Figures 15(a)–15(f) show contour plots of the charge den-

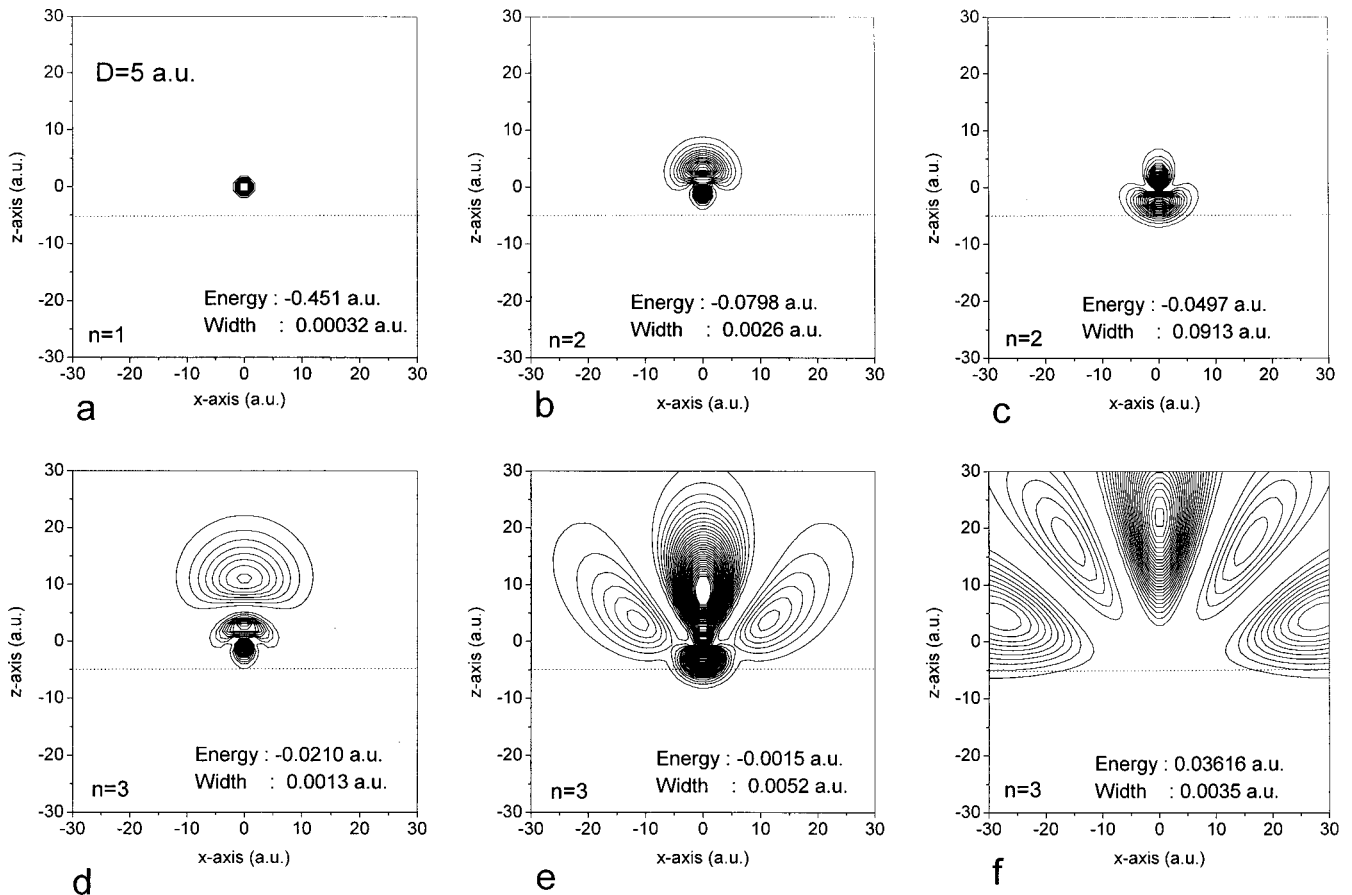


FIG. 15. Density associated with the (normalized) resonance wave functions of the asymptotic ($n=1$) to ($n=3$) manifolds at $D=5$ a.u. Only ($m=0$) states are shown.

sity for ($m=0$) states that asymptotically merge into the $n=1, 2,$ and 3 manifolds for an ion-surface distance of $D=5$ a.u. Both axes refer to the projectile frame and the dotted line marks the jellium edge. As can be seen, the asymptotic ($n=1$) state is not altered by the surface and exhibits a rather small width. The ($n=2$) manifold shows the typical Stark mixing: one state points towards the vacuum and has a small width while the second state points towards the metal surface, its width being about two orders of magnitude larger due to the larger overlap with the surface (similar to upfield and downfield Stark states). The ($n=3$) manifold splits into three states of small, medium, and large width. At small ion-surface distances states of the ($n=3$) manifold that have a large width (due to their overlap with the surface) tend to be promoted near the ionization threshold and mix with higher n manifolds, whereas states with a small width tend to keep their asymptotic Stark-like character.

V. SUMMARY AND CONCLUSIONS

Within the fixed-ion approximation, we have studied the electronic self-energy of hydrogenic ions interacting with a jellium metal surface. We have employed a model framework in which the jellium potential is assumed to be of step-functional form and in which the classical image potentials are approximately taken into account. This framework allows an efficient and accurate evaluation of the complex self-energy matrix in a large space of ionic basis states. Adiabatic energies and resonance widths of dressed ionic states which were determined from the eigenvalues of the full self-energy matrix were found to be in good overall agreement with results obtained previously from other nonperturbative methods. This shows that the electronic potential we use, while being of a somewhat simple form, is sufficiently realistic to describe the essential features of the ion-surface interaction.

In order to gain detailed insight into the effect of the various couplings acting among the ionic states, we have compared the energies gained from diagonalizing the full self-energy matrix to (1) energies obtained by taking into account the direct couplings only and to (2) the diagonal elements of the self-energy matrix. This comparison reveals the pronounced influence of the indirect couplings via the jellium states on the energies at intermediate and small ion-surface distances. The direct couplings are responsible, due to the dominating effect of the attractive jellium potential, for a strong lowering of the energies. This downward shift, however, is overcompensated by the indirect couplings through conduction band states, thereby leading to an overall

increase of the resonance energies. Accordingly, except for states located near or below the lower band edge, the indirect couplings as represented by the principal-part term in the self-energy matrix effectively act as a strongly repulsive potential on the ionic states. By successively enlarging the space of ionic basis states, we have studied the convergence properties of the self-energy method.

A number of further issues remain to be investigated in future work. Foremost among them is a precise estimate of the uncertainties introduced by adopting the Wigner-Weisskopf approximation in the evaluation of the self-energy. Possible improvements over this approximation, in particular the self-consistent solution of the nonlinear eigenvalue problem for the self-energy, are being studied [40]. In order to make the comparison to other nonperturbative calculations even more stringent, more refined forms of the electron-surface potential need to be taken into account in our calculations.

The resonance energies and dressed wave functions calculated in the fixed-ion approximation form an appropriate starting point for the dynamical treatment of slow ion-surface interactions within the rate-equation approach and the time-dependent close-coupling method. In the latter method, the self-energy acts as a (time-local) complex optical potential, and the dressed states are coupled by dynamical couplings induced by the motion of the ion relative to the surface. The optical-model close-coupling treatment of ion-surface interactions bears close resemblance to the dynamical treatment of slow ion-atom collisions, in which ‘‘quasi-molecular’’ states calculated at fixed ion-atom distance are employed in the expansion of the time-dependent scattering wave function. We are currently undertaking exploratory studies in which the applicability of the close-coupling method to ion-surface interactions is examined [40,42].

ACKNOWLEDGMENTS

We thank J. Burgdörfer for very fruitful discussions. U.T. acknowledges the hospitality of the University of Tennessee and the Oak Ridge National Laboratory during the early stages of this work. P.K. thanks the Hahn-Meitner-Institut Berlin for kind hospitality during his stay. This work has been supported by the Deutsche Forschungsgemeinschaft (DFG) through a grant for P.K. and by the Division of Chemical Sciences, Basic Energy Sciences, Office of Energy Research, U.S. Department of Energy. Computational efforts were greatly facilitated through Grant No. DMR-9413513 from the National Science Foundation.

-
- [1] M. Grether, A. Spieler, R. Köhrbrück, and N. Stolterfoht, *Phys. Rev. A* **52**, 426 (1995).
 - [2] J. Limburg, S. Schippers, I. G. Hughes, R. Hoekstra, R. Morgenstern, S. Hustedt, N. Hatke, and W. Heiland, *Nucl. Instrum. Methods Phys. Res. B* **98**, 436 (1995); *Phys. Rev. A* **51**, 3873 (1995).
 - [3] S. Winecki, C. L. Cocke, D. Fry, and M. P. Stöckli, *Phys. Rev. A* **53**, 4228 (1996).
 - [4] I. G. Hughes, J. Limburg, R. Hoekstra, R. Morgenstern, S. Hustedt, N. Hatke, and W. Heiland, *Nucl. Instrum. Methods Phys. Res. B* **98**, 458 (1995).
 - [5] F. W. Meyer, L. Folkerts, and S. Schippers, *Nucl. Instrum. Methods Phys. Res. B* **100**, 366 (1995).
 - [6] L. Folkerts, S. Schippers, D. M. Zehner, and F. W. Meyer, *Phys. Rev. Lett.* **74**, 2204 (1995).
 - [7] H. Winter, *J. Phys. Condens. Matter* **8**, 10149 (1996).
 - [8] C. Lemell, H. P. Winter, F. Aumayr, J. Burgdörfer, and F. Meyer, *Phys. Rev. A* **53**, 880 (1996).

- [9] J. W. Gadzuk, Surf. Sci. **6**, 133 (1967); **6**, 159 (1967).
- [10] M. Remy, J. Chem. Phys. **53**, 2487 (1970).
- [11] U. Thumm and J. S. Briggs, Nucl. Instrum. Methods Phys. Res. B **43**, 471 (1989).
- [12] U. Thumm and J. S. Briggs, Nucl. Instrum. Methods Phys. Res. B **40/41**, 161 (1989); **47**, 476 (1990).
- [13] U. Thumm, Ph.D. thesis, University of Freiburg, 1989.
- [14] U. Thumm, J. Phys. B **25**, 421 (1992).
- [15] U. Wille, Phys. Rev. A **45**, 3004 (1992).
- [16] U. Wille, Nucl. Instrum. Methods Phys. Res. B **67**, 132 (1992).
- [17] U. Wille, Nucl. Instrum. Methods Phys. Res. B **79**, 132 (1993).
- [18] U. Wille, Nucl. Instrum. Methods Phys. Res. B **90**, 295 (1994).
- [19] U. Wille, Surf. Sci. **307–309**, 874 (1994).
- [20] U. Wille, Phys. Rev. B **50**, 1888 (1994).
- [21] U. Wille, Nucl. Instrum. Methods Phys. Res. B **100**, 303 (1995).
- [22] P. Kürpick and U. Thumm, Phys. Rev. A **54**, 1487 (1996).
- [23] J. Burgdörfer, E. Kupfer, and H. Gabriel, Phys. Rev. A **35**, 4963 (1987).
- [24] J. Burgdörfer, in *Review of Fundamental Processes and Applications of Atoms and Ions*, edited by C. D. Lin (World Scientific, Singapore, 1993), p. 517.
- [25] R. Brako and D. M. Newns, Rep. Prog. Phys. **52**, 655 (1989).
- [26] A. T. Amos, K. W. Sulston, and S. G. Davison, Adv. Chem. Phys. **76**, 335 (1989).
- [27] A. G. Borisov, D. Teillet-Billy, and J. P. Gauyacq, Nucl. Instrum. Methods Phys. Res. B **78**, 49 (1993).
- [28] G. E. Makhmetov, A. G. Borisov, D. Teillet-Billy, and J. P. Gauyacq, Europhys. Lett. **27**, 247 (1994).
- [29] A. G. Borisov and U. Wille, Surf. Sci. **338**, L875 (1995); Nucl. Instrum. Methods Phys. Res. B **115**, 137 (1996).
- [30] A. G. Borisov, R. Zimny, D. Teillet-Billy, and J. P. Gauyacq, Phys. Rev. A **53**, 2457 (1996).
- [31] P. Nordlander and J. C. Tully, Phys. Rev. Lett. **61**, 990 (1988); Phys. Rev. B **42**, 5564 (1990).
- [32] P. Nordlander, Phys. Rev. B **53**, 4125 (1996).
- [33] D. A. Micha and E. Q. Feng, Comput. Phys. Commun. **90**, 242 (1994).
- [34] S. Deutscher, X. Yang, and J. Burgdörfer, Nucl. Instrum. Methods Phys. Res. B **100**, 336 (1995).
- [35] (a) S. Deutscher, X. Yang, J. Burgdörfer, and H. Gabriel, Nucl. Instrum. Methods Phys. Res. B **115**, 152 (1996); S. A. Deutscher, X. Yang, and J. Burgdörfer, Phys. Rev. A **55**, 466 (1997); (b) S. Deutscher and J. Burgdörfer (unpublished).
- [36] F. Martín and M. F. Politis, Surf. Sci. **356**, 247 (1996).
- [37] J. P. Hansen, Surf. Sci. **321**, L244 (1994).
- [38] J. Merino, N. Lorente, P. Pou, and F. Flores, Phys. Rev. B **54**, 10959 (1996).
- [39] J. C. Tully, Phys. Rev. B **16**, 4324 (1977).
- [40] P. Kürpick, U. Thumm, and U. Wille (unpublished).
- [41] P. J. Jennings, R. O. Jones, and M. Weinert, Phys. Rev. B **37**, 6113 (1988).
- [42] P. Kürpick, U. Thumm, and U. Wille, Nucl. Instrum. Methods Phys. Res. B **125**, 273 (1997).